Two-Dimensional Blade-Vortex Flow Visualization Investigation

E. R. Booth Jr.* and J. C. Yu†
NASA Langley Research Center, Hampton, Virginia

Results from a flow visualization study to examine the details of two-dimensional blade-vortex interaction are described. The study employed an oscillating airfoil to generate vortex filaments that were allowed to interact with an airfoil model, positioned in the flow to simulate a rotor blade section. Blade position in the flow was parametrically varied. Trajectory data indicate blade position measurably affects vortex trajectory, although this influence decreases rapidly with increasing vortex-to-blade spacing. In close proximity, optical data indicate that the blade significantly distorts the structure of the vortex during the encounter.

Nomenclature

c	= vortex generator chord length, 15.24 cm
C	= blade model chord length, 20.32 cm
d	= apparent vortex core diameter
d/C	= vortex core diameter to blade chord ratio
k	= reduced frequency, $k = \omega c/2U_\infty$
U	= vortex velocity in the X direction
U_∞	= freestream velocity
X	= distance downstream of vortex generator, m
X/C	= nondimensional X direction coordinate
Y	= distance from centerline of test section, m
Y/C	= nondimensional Y direction coordinate
Y_b/C	$= Y/C_{\text{vortex}} - Y/C_{\text{blade}}$

Introduction

BLADE-VORTEX interaction (BVI) has been identified as the source of a particularly annoying type of helicopter impulsive noise[1] that is likely to occur when the helicopter is in powered descent.[2] Although the acoustic formulation of BVI noise is fairly well developed, the complex aerodynamics required as the input to the acoustic formulation are seriously deficient.[1,3] In order to gain insight into the detailed aerodynamics of BVI, an experimental program was initiated at NASA Langley to study this complex phenomenon.

Blade-vortex interaction in helicopter rotors occurs when the tip vortex from a rotor blade is ingested by the rotor disk and comes into close proximity (or actually collides) with another rotor blade at some intersection angle determined by the operating conditions of the rotor and the azimuthal location of the encounter. This encounter causes an unsteady impulsive aerodynamic load on the rotor blade that is radiated as BVI noise. Widnall[4] linked the intersection angle of the encounter to the intensity of the acoustic pulse, such that, in the limiting case, if the axis of the vortex is parallel to the span of the rotor blade, the most intensive pulse is produced. Nakamura[5] reached a similar conclusion, but related his observations to the acoustic planform of the blade rather than the actual planform and also pointed out the importance of the leading edge of the rotor blade in the interaction process.

Experimentally, Hoad[6] demonstrated that the most intense BVI acoustic radiation is generated between 65 and 90 deg azimuth angle and 0.6-1.0 radius from the hub. This is supported by the earlier study of Tangler[7] in which the two BVI encounters most important in noise generation occurred at azimuth angles of 55 and 70 deg. Recent analytical work by Egolf and Landgrebe[8] on the structure of rotor wakes shows this region to contain trailing vortices in a nearly parallel orientation to the advancing rotor blade. However, the study concludes that more experimental work is needed concerning the detail of the close encounter between a rotor blade and a vortex filament.

In view of the above-mentioned analytical and experimental findings, it was decided that the experimental investigation should start with the limiting case of interest: two-dimensional blade-vortex interaction, defined as the particular BVI where the intersection angle between the vortex filament and the blade span is zero. The experiment is limited to low subsonic flows. It is felt that the particular experimental configuration used avoids the complexity involved with a rotor, yet preserves the important physical characteristics of BVI noise generation.

The experiment was designed to examine some of the details of the blade-vortex encounter that had not been previously studied in depth. Of particular importance are the vortex trajectory changes due to the presence of the blade and the distortion and dissipation of the vortex as a result of the encounter. The present experiment complements a parallel computational investigation of two-dimensional BVI reported by Hardin and Lamkin.[9]

Results from the initial part of the investigation based on the flow visualization data are presented in this paper.

Description of the Experiment

The study was conducted in the Quiet Flow Facility in the Langley Aircraft Noise Reduction Laboratory. The test arrangement used the low pressure air system as described in Ref. 10. A 0.30×0.46 m rectangular nozzle was used with side plates fitted to the long sides to form a two-dimensional test section. Test section velocity, monitored continuously by a pitot-static probe, was maintained at a nominal 6.1 m/s. The vortex generator consisted of a 15.24 cm chord NACA 0012 airfoil section spanning the test section, and driven by an electric motor to oscillate sinusoidally in pitch about its quarter chord at frequencies up to 30 Hz with a miximum amplitude of 10 deg. Kerosene smoke was injected into the flow from a small port located in the midspan trailing edge of the vortex generator airfoil. A stationary 20.32 cm chord NACA 0012 airfoil was placed downstream of the vortex generator to simulate a rotor blade for the vortex encounter. Photographic data was obtained using video and still photography through

Presented as Paper 84-2307 at the AIAA/NASA Ninth Aeroacoustics Conference, Williamsburg, VA, Oct. 15-17, 1984; received March 18, 1985; revision received Jan. 21, 1986.

*Research Engineer, Aeroacoustics Branch, Acoustics Division. Member AIAA.

†Assistant Head, Aeroacoustics Branch, Acoustics Division. Associate Fellow AIAA.

the large windows in the side plates. A strobe light assembly was positioned to illuminate the area between the side plates. An illustration and photograph of the test configuration are presented as Fig. 1.

The experiment employed several complex techniques: the generation of the vortex filaments, the phase-locked photography used to record the data, and the measurement of trajectory data. Each of these techniques are described in the following sections.

Description of the Vortex Generator

The vortex filaments studied were generated by a sinusoidally oscillating airfoil. It is well established that, at sufficiently large reduced frequency k, the wake behind an oscillating airfoil contains pairs of vortex filaments resembling a Karman vortex street.[11] With an airfoil oscillating in a two-dimensional test section, these vortex filaments can be used to represent the vortex filament in the correct orientation for two-dimensional blade-vortex interaction.

It is pertinent to point out that there exist some inherent limitations in the experimental method used. First, the vortex pairs cannot be considered to be exactly equivalent to an isolated tip vortex encountering a rotor blade on a helicopter rotor. Because the vortex filaments occur in pairs, they influence each other as a vortex street, likely a very stable configuration. Second, in the presence of a blade, the spacing between the filaments becomes important: The blade can be said to have an isolated encounter only if the spacing between the filaments is greater than the blade model chord. Such a requirement may be in conflict with the need for a well-defined vortex and, consequently, the condition for an isolated encounter is not always met. Finally, certain possibly important aspects of the real encounter case are not fully simulated, such as the effects of rotor rotation, compressibility, and turbulence ingestion. However, the present investigation does retain the geometry and time dependency of the real situation.

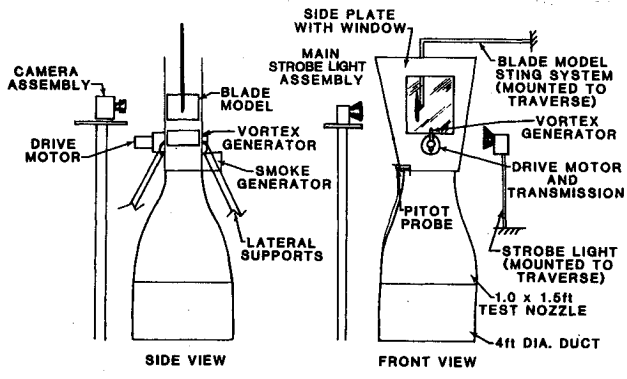

Fig. 1 Test apparatus.

Description of Phase-Locked Photography Technique

Because the flowfield was periodic with the vortex generator motion, it was possible to use the phase angle of the oscillation to drive the strobe lights and, at a selected phase angle, the motion of the flow could be optically frozen. This made possible the use of phase-averaged photography where several images occurring at the same phase angle in successive cycles were combined on one photographic frame. Among the advantages of this technique are the capability of recording extremely thin traces of smoke by building up the photographic image for several cycles, and the ability to gather the data as a function of oscillation phase angle; a convenient time reference.

Measurement of Trajectory Data

The trajectory data obtained in this study were measured from photographic data. Since the photographic data were obtained as a function of oscillation phase angle, measurement of the location of the center of the respective vortex cores in a series of photographic frames yields the trajectory of the vortex cores during the oscillation period. In close-encounter cases, where the vortex core center was not discernible, the largest recognizable remnant of the vortex was tracked.

Locations from the photographic records were measured using a digitizing tablet and associated software. The overall spatial accuracy is on the order of 0.25 cm in both X and Y coordinates.

Experimental Results

The experiment was divided into two cases. 1) The free-wake case (wake produced by the sinusoidally oscillating vortex generator without the blade in the flow) was used to determine the effects of operating conditions on the structure of the wake. The free-sinusoidal-wake case also served as a baseline case for the experiment. 2) The two-dimensional BVI case consisted of placing the blade model in the vortex wake. The interactions of the wake vortex filaments with the blade were observed as a function of blade position.

Free Wake

The free-sinusoidal-wake case was used to determine the optimum operating conditions of the experimental apparatus. Analyses available in the literature, such as the one by Katz and Weihs,[11] pointed out the necessity of high reduced frequency for good development of the vortex filaments in the wake. Although reduced frequency is directly proportional to

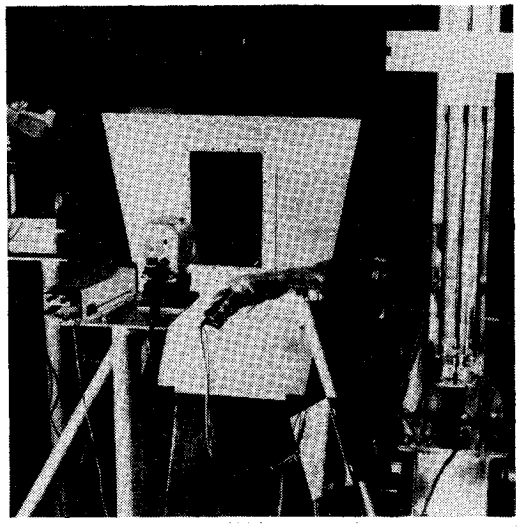

Fig. 2 Free sinusoidal wake.

vortex generator oscillation rate, it is inversely proportional to test section freestream velocity. Thus, maximum reduced frequency attainable is defined by the minimum controllable test section velocity and the maximum vortex generator oscillation rate. Unfortunately, high reduced frequency also decreases the distance between adjacent vortex filaments, not desirable for simulating an "isolated encounter" where the spacing of adjacent filaments should be large compared to the blade chord length. An in-house computational analysis of the aerodynamics of the vortex generator suggested that well-developed vortex filaments could be produced at lower reduced frequencies by increasing the amplitude of the oscillation. The wake produced by the sinusoidally oscillating vortex generator at 30 Hz with an amplitude of 10 deg operating in a freestream velocity of 6.1 m/s was selected as the baseline case for this investigation. These operating conditions produce a wake with one blade chord length between vortex filaments of like sign.

A typical photograph of the baseline free sinusoidal wake is presented as Fig. 2. Notice the alternating vortex filaments in the wake. Although the streamers of smoke connecting the vortex filaments are also a part of the sinusoidal wake, the vortex filaments themselves are the portion of the wake that is of interest. The vortex filaments alternate in sign with the vortices of opposite sign traversing different, staggered paths. The upper vortex filaments (as seen in the photograph) circulate in a counterclockwise direction and are negative vortex filaments, while the lower filaments, with clockwise circulation, are positive vortex filaments.

The trajectories of the vortex filaments in the free sinusoidal wake are presented in Fig. 3. The origin of the coodinate system is located at the neutral position of the vortex generator. Distances in the test section are normalized by the blade chord to be consistent with the remainder of the data. Notice that although, intuitively, the wake produced by the symmetric sinusoidal oscillation should be symmetric, this is not the case. In fact, it appears that the trajectories of the two filaments tend to converge to a spacing of $\Delta Y/C$:$\Delta X/C$ on the order of 0.20 with $\Delta Y/C$ taken as the distance between the two trajectories and $\Delta X/C$ as the distance between two filaments of the same sign. This compares with the spacing of 0.281 for the Karman vortex street.[12] Apparently, the asymmetry in the vortex trajectories is a result of the two families of vortex filaments rearranging themselves into a more stable configuration. In Fig. 4, convection velocity data of the two vortex filaments are presented. Velocity data were computed by differentiating trajectory data with respect to time. Unfortunately, this process magnifies measurement error, therefore the trajectory data was fitted with a least-squares curve before it was differentiated. As a result, some of the detail of the convection velocity was lost because this detail is of the same order of magnitude as the measurement error. The resulting data, although necessarily approximate, does indicate the general trends of vortex filament velocity.

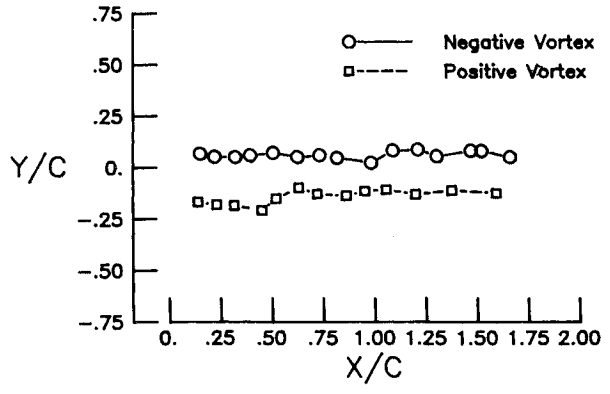

Fig. 3 Trajectory of two vortex filaments in the free sinusoidal wake.

Notice that both vortex filaments begin by traveling at less than the freestream velocity. This reflects the fact that the vortex filament is formed relatively near the trailing edge of the vortex generator. As the filament moves away from the vortex generator, it accelerates to a velocity somewhat greater than that of the freestream. A possible explanation for this may lie in the way the vortex filaments rearrange themselves into the vortex street-like configuration. After the filament accelerates to this higher-than-freestream velocity it begins to decelerate back to the freestream velocity. This occurs as the filament degenerates into an ill-defined structure that is whisked away by the freestream velocity.

Another feature of the free wake relevant to BVI is the relative size of the vortex core to the chord length of the blade. In Fig. 2, it appears that the size of the vortex grows as it traverses the test section. The apparent core diameter of the negative vortex filament is plotted as a function of test section position in Fig. 5. Data for the positive vortex filament is similar. The apparent core boundary is taken as that radial position at which the entrained smoke is densest. Since this boundary is approximate, some data scatter is expected and the data were faired with a second-order least-squares curve fit to emphasize the trend. Notice that the core size increases with the square of downstream position, hence, time, rather than proportional to the square root of time, as Prandtl's analysis[13] predicts for an isolated vortex. A possible explanation for the accelerated dissipation of the vortex filaments is that each filament imposes a shear flow on every other filament, which tends to tear the vortex filaments, causing premature dissipation. Hardin and Lamkin[9] saw a similar mechanism at work in their computational study except that the shear flow on the vortex filament was imposed by the circulation about the airfoil. The change in size of the vortex filament with position in the test section has implications in the geometric scaling of the

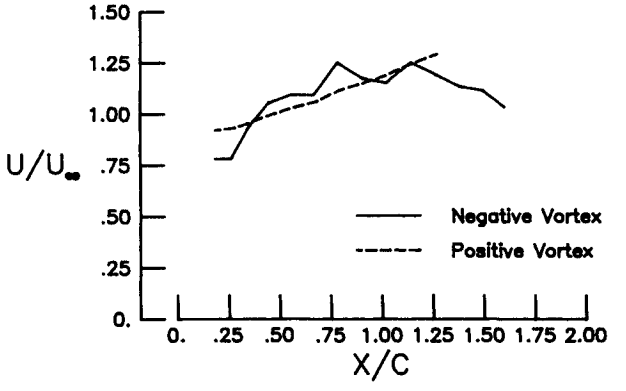

Fig. 4 Convection velocity of vortex filaments in the free sinusoidal wake as a function of vortex position.

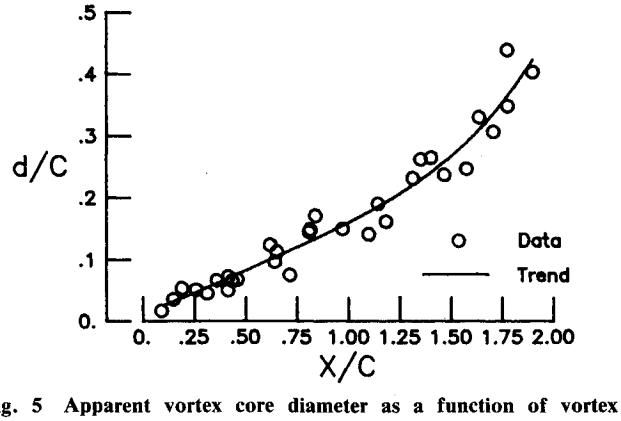

Fig. 5 Apparent vortex core diameter as a function of vortex position.

two-dimensional BVI case, in that, by placing the leading edge of the blade at the $X/C=0.75$ location, the ratio d/C is equal to 0.12. This compares well with a generally accepted value of d/C relevant to BVI of approximately 0.10.[14]

Two-Dimensional BVI

Although the free sinusoidal wake is an interesting object of study in itself, the main purpose of this investigation is the examination of interactions between the sinusoidal wake and a blade model in the flow. Figure 6 is a typical photograph of the blade immersed in the sinusoidal wake. In this particular photograph, the vortex filaments appear to be solidly filled in, due in part to the smoke concentration, which was rather dense for this particular photograph and also the phase-averaged photography which blended several partially filled vortex cores into a single, solid image. Blade position is completely defined by the X, Y location of the blade leading edge and blade angle of attack. Due to scaling considerations, the leading edge of the blade was maintained at $X/C=0.75$. Blade positions tested included excursions in the Y direction up to $0.375C$ and angles of attack of 0, 5, and 10 deg. Thus, three major points to be examined are the effect of placing the blade in the flow, the effect of vertical (Y direction) displacement of the blade, and the effect of angle of attack on the trajectory of the vortex filaments. Additionally, the nature of the close encounter case, where vortex distortion is important, is discussed.

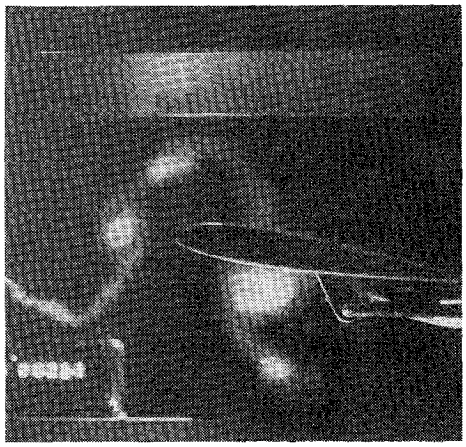

Fig. 6 Blade model in sinusoidal wake.

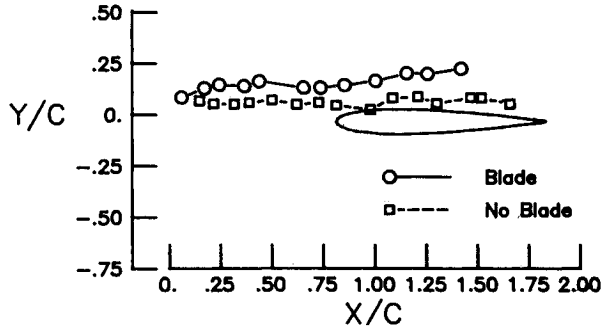

a) Negative vortex filament.

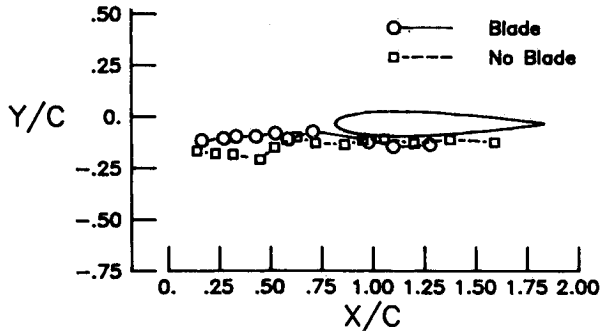

b) Positive vortex filament.

Fig. 7 Effect of blade presence on vortex trajectory.

In order for this experiment to produce information about blade-vortex interaction, the BVI effects should be stronger than the vortex-vortex interactions that cause asymmetry in the wake. Thus, there must be observable differences in the wake structure due to the presence of the blade in the sinusoidal wake. Figure 7 compares the trajectory of the negative vortex filament and positive vortex filaments, respectively, with the blade in the flow to the free-wake case. Notice that the trajectory of the negative vortex filament is generally displaced upward due to the presence of the blade. This displacement effect is the expected result due to blade thickness. Although not as pronounced in Fig. 7b, the same type of effect is present. Notice in Fig. 7b, that the trajectory of the positive filament is smoother upstream of the blade than the free-wake case. The trajectory data in Fig. 7a also show a smoothing of filament trajectory in the presence of the blade. These observations imply that the blade-vortex interaction dominates the flowfield while the vortex-vortex interaction observed in the free-wake case is weaker.

The effect of the blade position with respect to the vortex wake is presented in Fig. 8. Although, in the actual experiment, the airfoil itself was moved, the vortex trajectory data in Fig. 8 are referenced to blade leading-edge position, thus Y_b/C is the vortex position in the Y direction relative to the blade leading edge. In Fig. 8a, the $Y_b/C=0$ case shows a reflex in vortex trajectory away from the blade. In the $Y_b/C=0.375$ case, the reflex is almost negligible and for the $Y_b/C=-0.375$ case, the reflex is, as may be expected, in the opposite direction, again away from the blade. Similar trends are evident in Fig. 8b, in fact, the $Y_b/C=0.375$ case appears

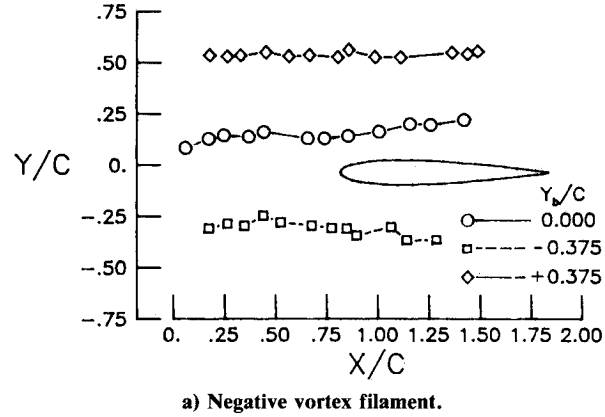

a) Negative vortex filament.

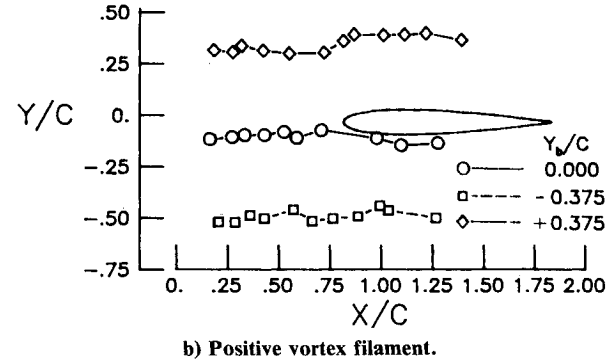

b) Positive vortex filament.

Fig. 8 Effect of blade vertical displacement on vortex trajectory.

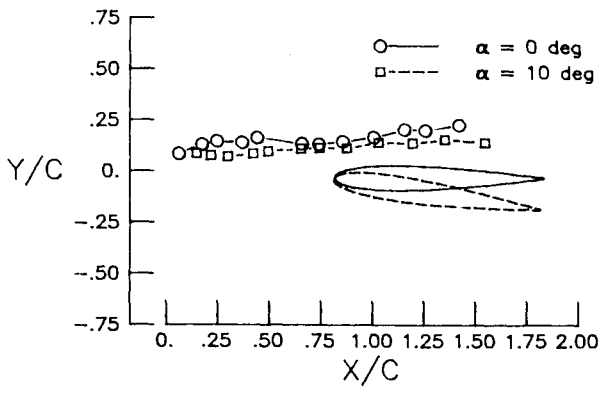

a) Negative vortex filament.

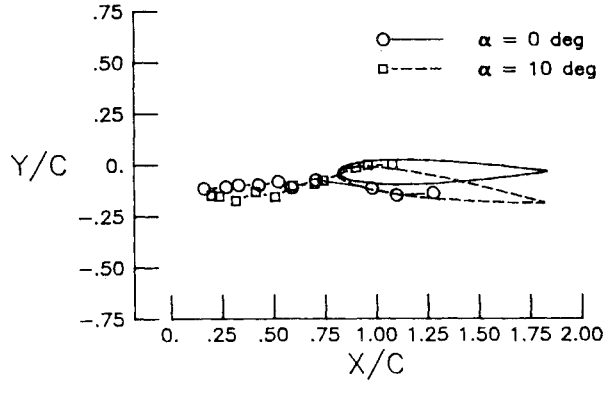

b) Positive vortex filament.

Fig. 9 Effect of blade loading on vortex trajectory.

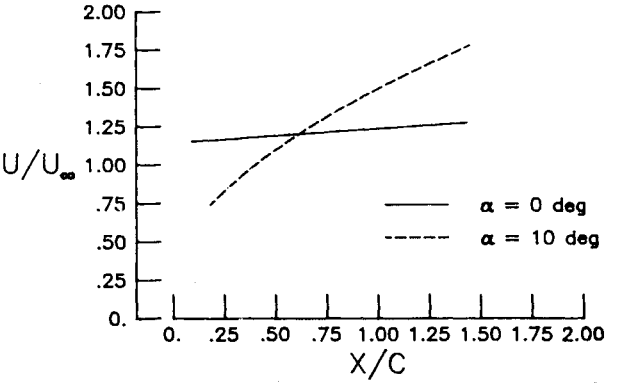

a) Negative vortex filament.

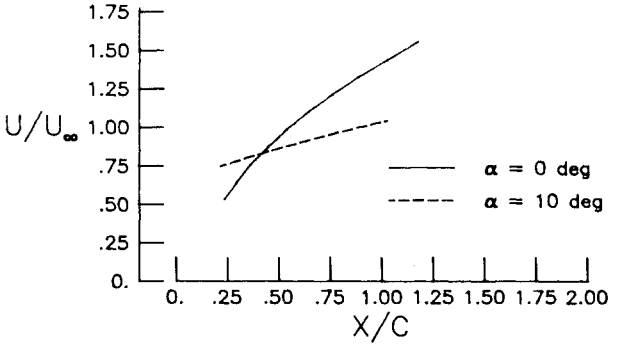

b) Positive vortex filament.

Fig. 10 Effect of blade loading on vortex convection speed.

to be very similar to the free-wake case. Apparently, the influence of the airfoil on the trajectory of the vortex filaments decreases rapidly with increasing separation distance.

Blade loading, due to changes in blade angle of attack, also has observable effects on vortex trajectory. The trajectories of the respective filaments are presented in Fig. 9 for the cases where blade angle of attack equals 0 and 10 deg. In Fig. 9a, it is evident that the trajectory of the negative vortex is closer to the blade for the $\alpha = 10$ deg case. Figure 9b shows that the vortex trajectory ahead of the blade is lower for the $\alpha = 10$ deg case than for the 0 deg case. Although, in Fig. 10b, it appears that the positive vortex filament travels beneath the blade for the 0 degree case and above for the 10 deg case, a close examination of the original photographic records indicates that as the vortex filament approached the blade in both cases, it split and traversed both sides of the blade, as described below. During measurement of the data the largest remnant of the vortex structure was tracked, so the change in vortex trajectory for this close encounter case is not quite as clear cut as the trajectory data indicate.

Figure 10 contains the convection velocities derived from differentiating the data presented in Fig. 9 with respect to time. As for the free-wake case, these data are approximate and can be used to examine only gross trends of the data. In Fig. 10a, the velocity of the negative vortex filament is increased by the blade loading as would be expected for a particle that travels above a loaded blade. In Fig. 10b, the opposite is seen to be true for the positive vortex filament, which convects slower for the loaded blade case. Thus, the effect of blade loading on vortex filament trajectories is similar to the effects expected for a particle in the flow near a loaded airfoil: Trajectories above the blade are drawn closer to the blade and accelerated, while trajectories beneath the blade are decelerated.

Although the phase-locked photographs were useful for quantifying the trajectory of the vortices as they encountered the blade, the slow-scan video records proved to be valuable in

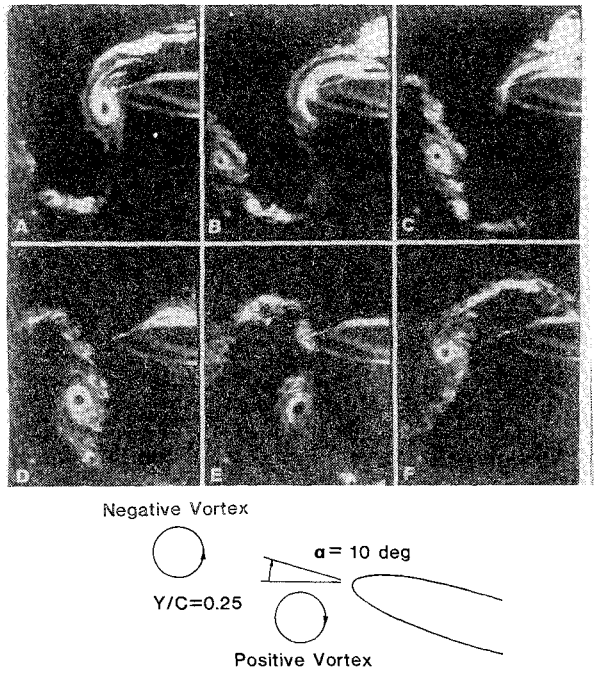

Fig. 11 Interaction of wake vortices with the blade at $Y/C = 0.25$.

observing the fine detail of the interaction process. Figures 11 and 12 are photographs taken from the video records and illustrated the interaction of an incident vortex with the blade in two of three interaction zones. The three interaction zones are the deflection zone, where the main characteristic of the interaction is a deflection of the vortex trajectory away from the blade; the distortion zone, where the structure of the vortex is distorted by the encounter; and the collision zone, where the vortex core actually collides with the blade. In both figures the blade is at 10 deg angle of attack.

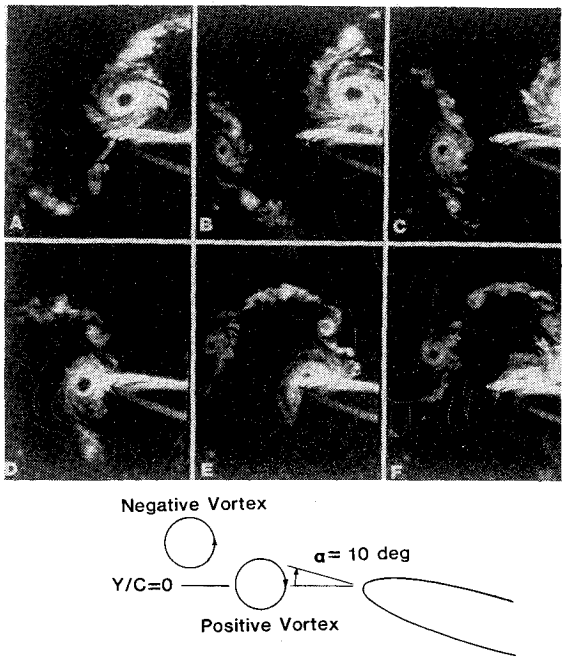

Fig. 12 Interaction of wake vortices with the blade at $Y/C=0.00$.

In Fig. 11, the interaction of the vortices in the wake with the blade are recorded for the deflection zone case with respect to the positive vortex. The blade is positioned at $X/C=0.75$, $Y/C=0.25$. Figure 11a shows the negative vortex in the instant before it collides with the blade. Figure 11b shows the separation zone induced on the upper surface of the airfoil by the negative vortex as the vortex core rolls underneath the blade leading edge in a distortion zone encounter. Note the severe elongation of the negative vortex core. The positive vortex appears in the left side of the frame. Figure 11c illustrates the advance of the positive vortex as the separation region induced by the negative vortex clings to the upper surface of the blade. Figure 11d shows the positive vortex continuing to advance toward the blade while the core size of the vortex expands. As the positive vortex reaches the blade (Fig. 11e), the core becomes oval in shape and is deflected away from the blade. The positive vortex, however, remains substantially organized as it passes underneath the blade, as shown in Fig. 11f; note the appearance of the negative vortex as the cycle closes. In this deflection zone encounter, the positive vortex structure is relatively undisrupted while its trajectory is altered by the blade.

In Fig. 12, the blade has been moved to the centerline of the test section. The flattening of the negative vortex core is illustrated in Figs. 12a and 12b, as the vortex passes over the blade in a distortion zone encounter. The positive vortex enters the photographic frame in Fig. 12b with a core size noticeably greater than illustrated in Figs. 11a and 11b. The expansion of the vortex core continues (Figs. 12c and 12d), as the vortex advances toward a collision zone encounter (Fig. 12e). In Fig. 12e, the positive vortex core is shown to split into two smaller vortex cores, one of which passes over the blade, the other beneath. The positive vortex pair is then shown to cling to the blade leading edge, Fig. 12f. This deceleration of the positive vortex core in the collision zone encounter is believed to be the major noise producing mechanism for low-speed BVI noise.[9]

Conclusions

Blade-vortex interaction (BVI) is a complex phenomenon to simulate. A partial simulation that avoids the complexities of a rotor system but preserves important physical characteristics of BVI noise production has been reported. Although limited to low subsonic flow velocities, the technique geometrically models the most intense case of BVI.

Vortex filaments were produced by oscillating an airfoil at a reduced frequency sufficiently high to insure the formation of well-defined vortex structure, although the spacing between adjacent vortices is not large enough to simulate an isolated encounter.

A systematic study of the changes to the vortex wake due to the presence of a blade immersed in the wake showed that the structure of the wake is modified as a function of blade position. The presence of a blade in the flow and the consequent blade-vortex interaction was shown to dominate the vortex-vortex interaction noted in the free wake. Blade influence on vortex trajectory was shown to decrease rapidly with blade-vortex spacing. Changes in blade loading were observed to influence vortex trajectory as if the vortex filament was a particle traveling with the flow in the nearfield of an airfoil. Vortex filament distortion was shown to be important for the close encounter case, and should be allowed for in any analytical treatment of this phenomenon.

Future work on two-dimensional BVI will concentrate on the effects of vortex proximity on airfoil loading, and development of experimental techniques to provide a well-defined "isolated" BVI.

References

[1]George, A. R., "Helicopter Noise: State-of-the-Art," *Journal of Aircraft,* Vol. 15, Nov. 1978, pp. 707-715.

[2]Schmitz, F. H., Boxwell, D. A., Lewy, S., and Dahn, C., "Model-to-Full-Scale Comparisons of Helicopter Blade-Vortex Interaction Noise," *Journal of the American Helicopter Society,* Vol. 29, No. 2, pp. 16-25

[3]Schmitz, F. H. and Yu, Y. H., "Helicopter Impulsive Noise: Theoretical and Experimental Status," presented at the International Symposium on Recent Advances in Aerodynamics and Aeroacoustics, Stanford Unversity, Stanford, CA, August 1984.

[4]Widnall, S., "Helicopter Noise Due to Blade-Vortex Interaction," *Journal of the Acoustical Society of America,* Vol. 50, No. 1, Pt. 2, pp. 354-365.

[5]Nakamura, Y., "Prediction of Blade Vortex Interaction from Measured Blade Pressure," presented at the 7th European Rotorcraft Powered Lift Forum, 1981.

[6]Hoad, D. R., "Helicopter Model Scale Results of Blade-Vortex Interaction Impulsive Noise as Affected by Tip Modification," presented at the 36th Annual Forum of the American Helicopter Society, Washington, DC, May 1980.

[7]Tangler, J. L., "Schlieren and Noise Studies of Rotors in Forward Flight," presented at the 33rd Annual Forum of the American Helicopter Society, Washington, DC, May 1977.

[8]Egolf, T. A. and Landgrebe, A. J., "Helicopter Rotor Wake Geometry and Its Influence in Forward Flight, Volume 1—Generalized Wake Geometry and Wake Effect on Rotor Airloads and Performance," NASA CR-3726, Oct. 1983.

[9]Hardin, J. C. and Lamkin, S. L., "Aeroacoustic Interaction of a Distributed Vortex with a Lifting Joukowski Airfoil," AIAA Paper 84-2287, Oct. 1984.

[10]Hubard, H. H. and Manning, J. C., "Aeroacoustic Research Facilities at NASA Langley Research Center," NASA TM-84585, March 1983.

[11]Katz, J. and Weihs, D., "Behavior of Vortex Wakes from Oscillating Airfoils," *Journal of Aircraft,* Vol. 15, Dec. 1978, pp. 861-863.

[12]Schlichting, H., *Boundary Layer Theory,* McGraw-Hill Book Co., New York, 6th ed., 1968, pp. 30-31.

[13]Prandtl, L., "The Mechanics of Viscous Fluids," *Aerodynamics Theory,* Vol. 3, edited by W. F. Durand, Durand Reprinting Committee, California Institute of Technology, Pasadena, CA.

[14]Rorke, J. B., Moffitt, R. C., and Ward, J. F., "Wind Tunnel Simulation of Full Scale Vortices," presented at the 28th Annual National Forum of the American Helicopter Society, Washington, DC, May 1972.